Carving Plasmon Modes in Silver Sierpiński Fractals - Supplementary Information

Isobel C. Bicket,[*,†] Edson P. Bellido,[†] Danielle M. McRae,[‡] François Lagugné-Labarthet,[*,‡] and Gianluigi A. Botton[*,†,¶]

†*McMaster University, 1280 Main Street West, Hamilton, ON, Canada, L8S 4L8*

‡*The University of Western Ontario, 1151 Richmond Street, London, ON, Canada, N6A 5B7*

¶*Canadian Light Source, 44 Innovation Boulevard, Saskatoon, SK, Canada, S7N 2V3*

E-mail: bicketic@mcmaster.ca; flagugne@uwo.ca; gbotton@mcmaster.ca

SI Pages: S1 - S25

SI Figures: S1 - S16

The Babinet Principle applied to G0 and iG0 Antennas

It is expected that aperture antennas, compared to solid antennas, should have a similar response in energy to orthogonal fields. If the dipole mode of a solid rectangular antenna is excited by vertically (horizontally) polarized light, the dipole mode of the aperture antenna responds to horizontally (vertically) polarized light.[1] The excitation in the aperture antenna can be considered equally as the excitation of a magnetic dipole moment in the same direction as the electric dipole of the solid complementary antenna, created by the circulation of ring currents around the edges of the aperture.[1,2] Since the G0 triangles of interest in this work have degenerate responses to horizontally and vertically polarized incident light, the inverse triangles (iG0) are expected to respond to both vertically and horizontally polarized light equivalently. EELS is a polarization-insensitive technique, so cannot directly pick up the different responses to orthogonally polarized light in solid and aperture antennas. However, EELS is sensitive to the near field of the surface plasmon resonance (SPR) mode and detects the change in orientation of the dipolar mode, as seen by Rossouw and Botton,[3] causing the EELS maps of the solid and inverse structures to appear complementary to each other.

Although the G0 and iG0 structures may be expected to show EELS peaks at the same energy, experimentally, there is no clear trend when comparing different sizes of G0 and iG0 structures (Fig. S1). Some are blueshifted (by almost 200 meV, Fig. S1(b)), others are redshifted by approximately 100 meV (Fig. S1(c)), and some, the largest pair of complementary structures fabricated in this work, have dipole peaks with only a difference of 30 meV between G0 and iG0 dipolar modes (Fig. S1(d)). There are many possible factors which can cause shifts in energy between the solid and inverse triangles. The Babinet principle, mathematically, requires the assumption that the conducting medium of the antenna is a perfectly thin, perfectly conducting film; neither of these assumptions are strictly true for the case of SPR antennas, so the Babinet principle should only be applied under the knowledge that it is only an approximation and rigorous agreement should not be expected.

The simulated peaks show a consistent small blueshift between G0 and iG0 (Fig. 1(a)),

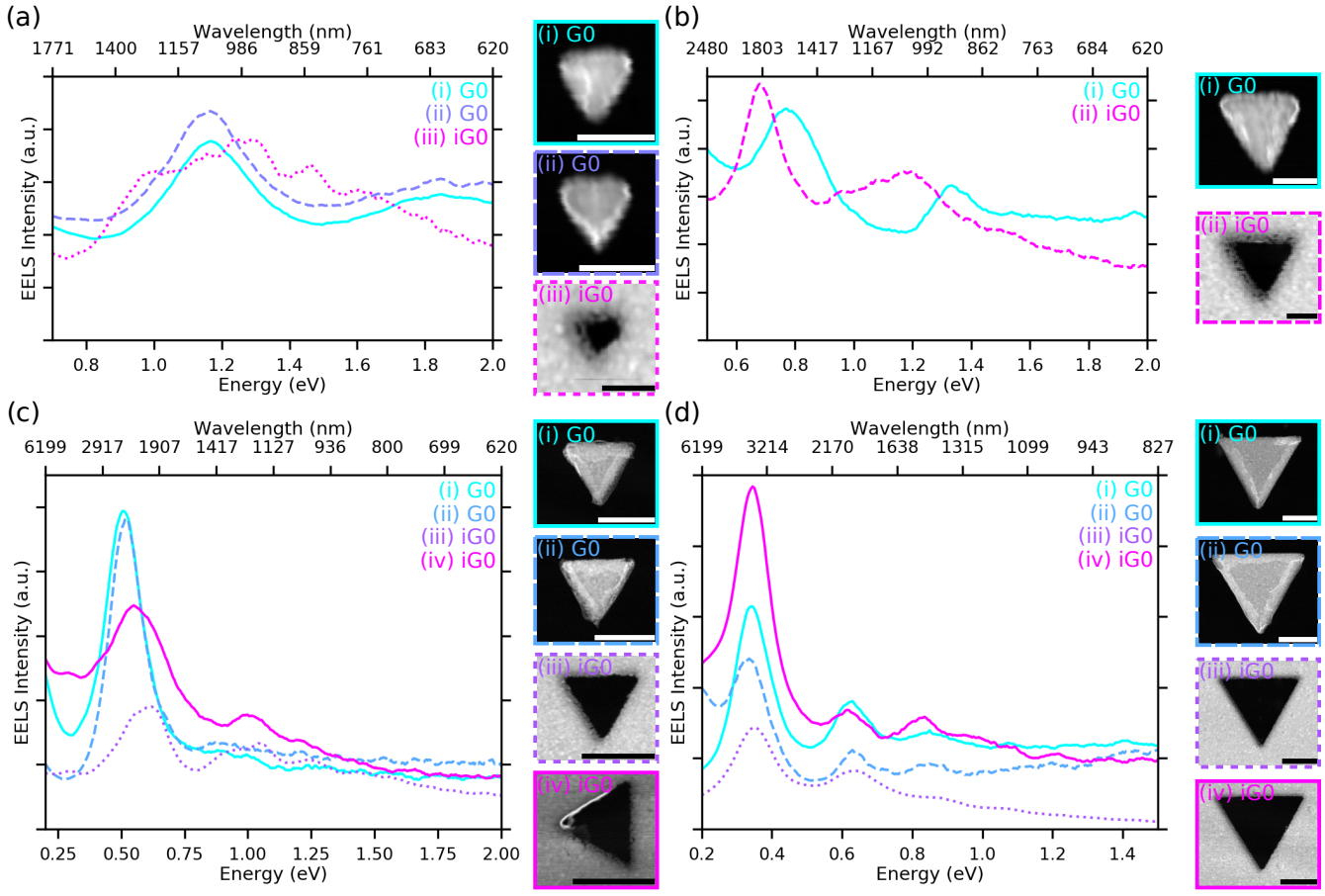

Figure S1: Dipole peak in EELS spectra and HAADF images for (a) triangles of approximately 150 nm (scalebars are 150 nm); (b) triangles of side length approximately 285 nm (scalebars are 150 nm); (c) triangles of side length approximately 550 nm (scalebars are 500 nm); and (d) triangles of side length approximately 1100 nm (scalebars are 500 nm).

which may be attributed to the effect of the SiN substrate.[4,5] The G0 prism and iG0 aperture have different field configurations: in the G0 prism, the dipolar field primarily surrounds the solid triangle, while in the iG0 aperture, the electric fields traverse the inverse triangle; the presence of the 50 nm thick SiN membrane may cause different energy shifts because of these differences in field configuration. Considering the variation in the experimental data, it may be concluded that the fabrication quality of each of these structures has a dominant effect on the relative peak energies.[6] Although the same method of fabrication was used for both G0 and iG0, the defects which occur most commonly are different. It may be observed, upon examination of the HAADF images (Fig. S1), that there is often a flap of material along the edges from the coating and lift-off process, particularly in G0 structures. This material is visible as a region of higher brightness around the edges of the triangle. With the iG0 apertures, this does not occur as frequently and the edges appear to be much more well-defined, although there is a thickness gradient of silver from the bulk film towards the aperture edges instead of an abrupt interface, due to shadowing during Ag deposition. Despite this gradient, the edges of the iG0 aperture are often much cleaner than those of a G0 prism of the same size. The number of modes visible along the edges of each of these structures highlights this point. For example, in Fig. 1(b,c) in the main text, more higher order edge modes are visible on the iG0 structure compared to the same size G0 structure. On the smaller structures, there is also more deviation in the peak energy between the two structures. Fabrication defects also explain why the trend is not consistent between different pairs of solid and inverse triangles, since these defects are not controlled or consistent at different length scales.

FDTD Calculations of iG0, G0, and G1

The following figures (Fig. S2 - S11) show simulated electric and magnetic field vectors at the indicated peak energy for horizontally and vertically polarized light for series of G0 and G1 triangles with increasing aperture size. The fields were calculated at a small distance above the Ag surface in vacuum. The electric and magnetic fields are presented for the two lowest energy optical peaks (both peaks are pairs of degenerate modes) of a triangular aperture in a continuous film (spectra (ix) in Fig. 3(c)) in Figs. S2 and S3. The electric and magnetic fields for the two lowest energy peaks of a solid G0 triangle (spectra (i) in Fig. 3(c)) are presented in Figs. S4 and S5. The following plots show the electric field vectors for the two lowest energy peaks (see spectra (ii) in Fig. 3(c)) of a 285 nm G1 fractal with a small central aperture (73 nm) (Fig. S6, S7); a 285 nm G1 fractal (see spectra (iii) in Fig. 3(c)) with a large aperture (142.5 nm, with 10 nm conductive channels) (Figs. S8, S9); and a 285 nm G1 fractal with no conductive coupling (see spectra (vi) in Fig. 3(c)) in Figs. S10, S11. For all plots, polarization of the excitation light is given by the green arrow. Streamlines indicate (x, y) field components and colours indicate the z component of the field for each plot.

Increasing the size of the central aperture reduces the size of the conductive channels between nanostructures, but reduces the net dipole moment and impairs the efficiency of coupling to light. Once the conductive channel is broken, as discussed in the main text (Fig. 3(c)(v, vi)), there is a sudden transition: charge cannot flow between G0 parent units and the structure no longer supports a net dipolar moment across the whole structure. The central aperture can no longer support aperture modes, which rely on charge flowing around the aperture corners. The transition is very abrupt and serves to emphasize the importance of conductive coupling between G0 parent units in higher order fractal generations.

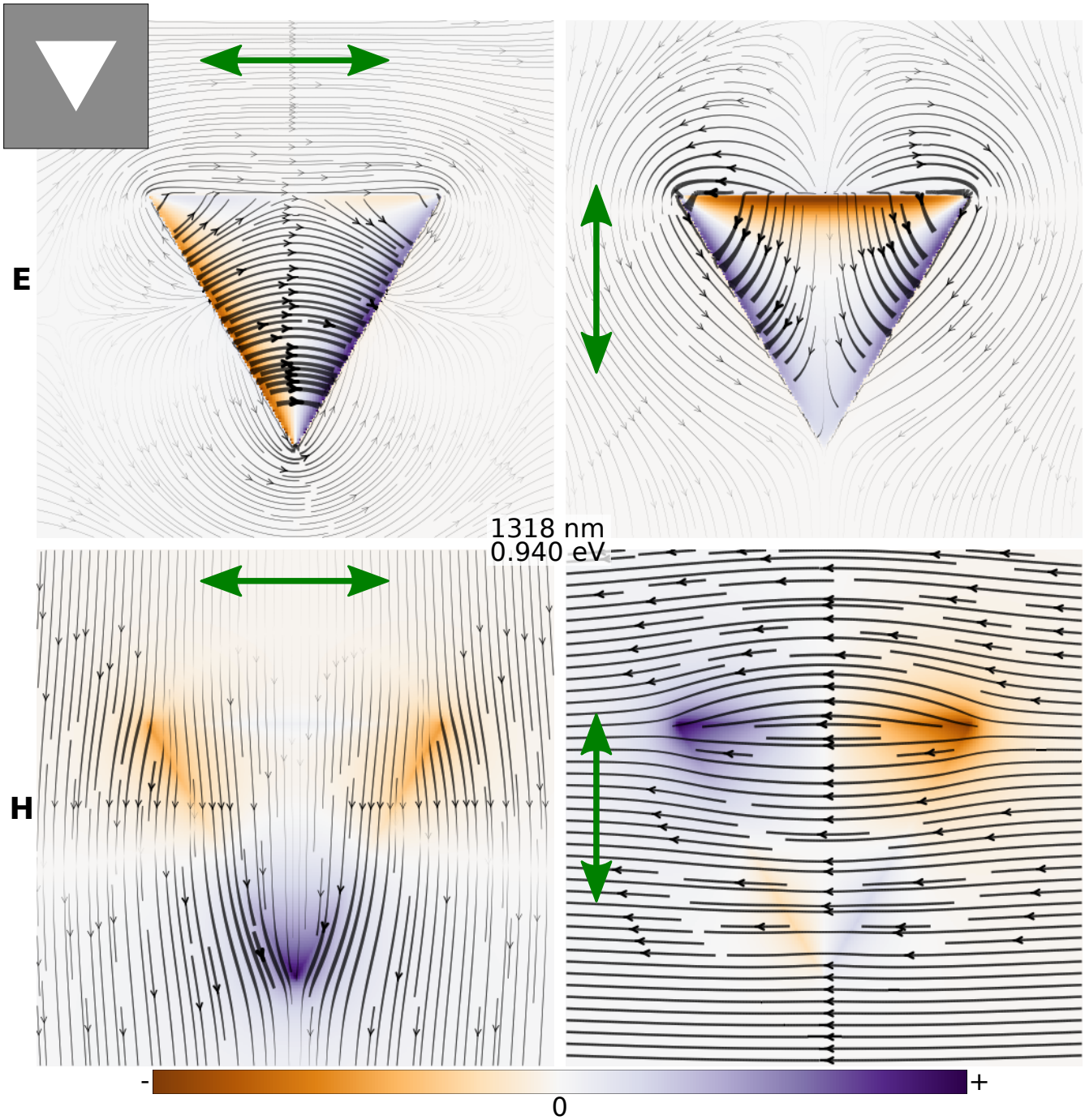

Figure S2: Simulated electric (**E**) and magnetic (**H**) fields for a plane just above the surface of the metal for a triangular aperture in an infinite metal film (iG0 structure) at 0.94 eV (1318 nm).

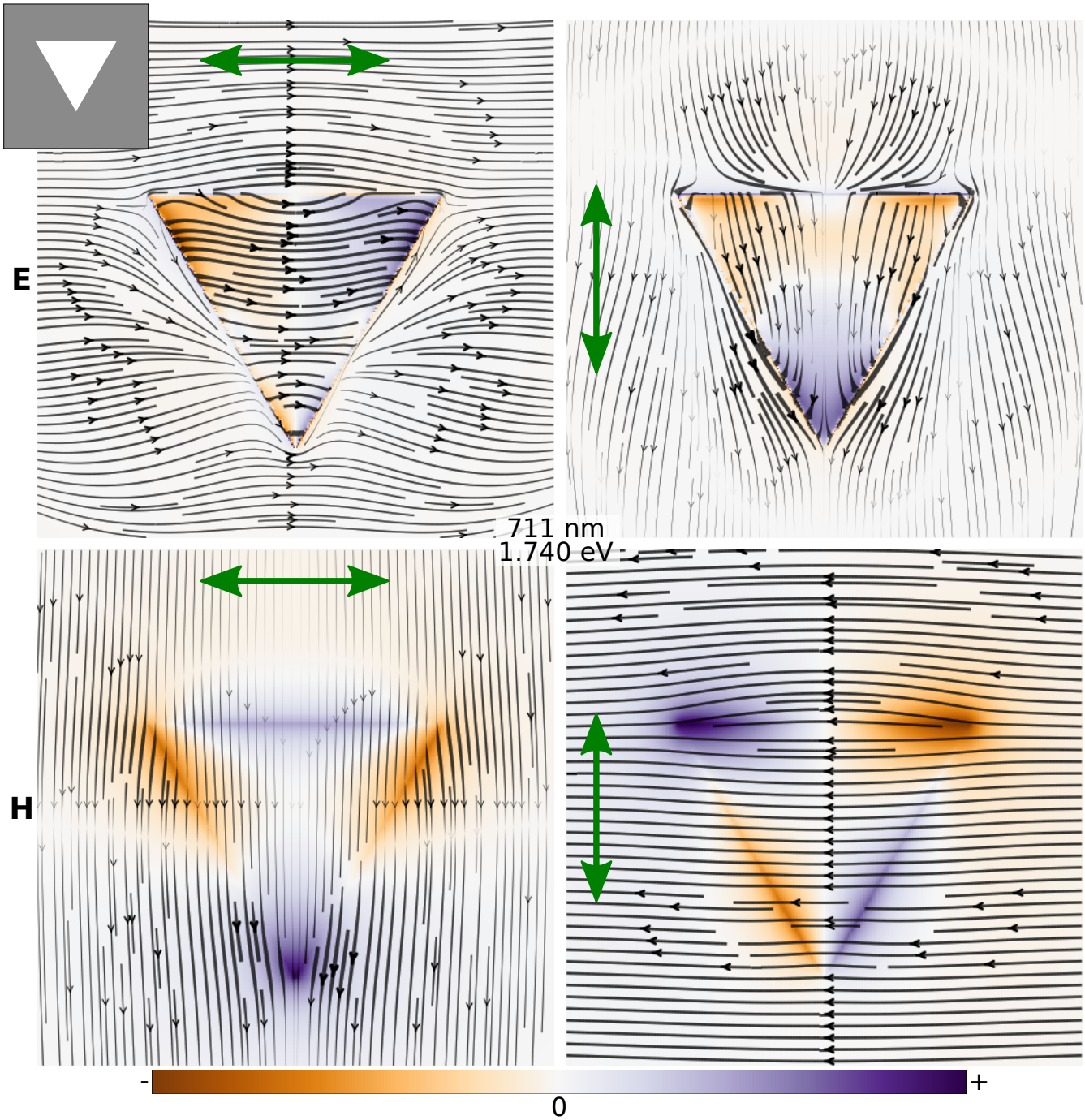

Figure S3: Simulated electric (**E**) and magnetic (**H**) fields for a plane just above the surface of the metal for a triangular aperture in an infinite metal film (iG0 structure) at 1.74 eV (711 nm).

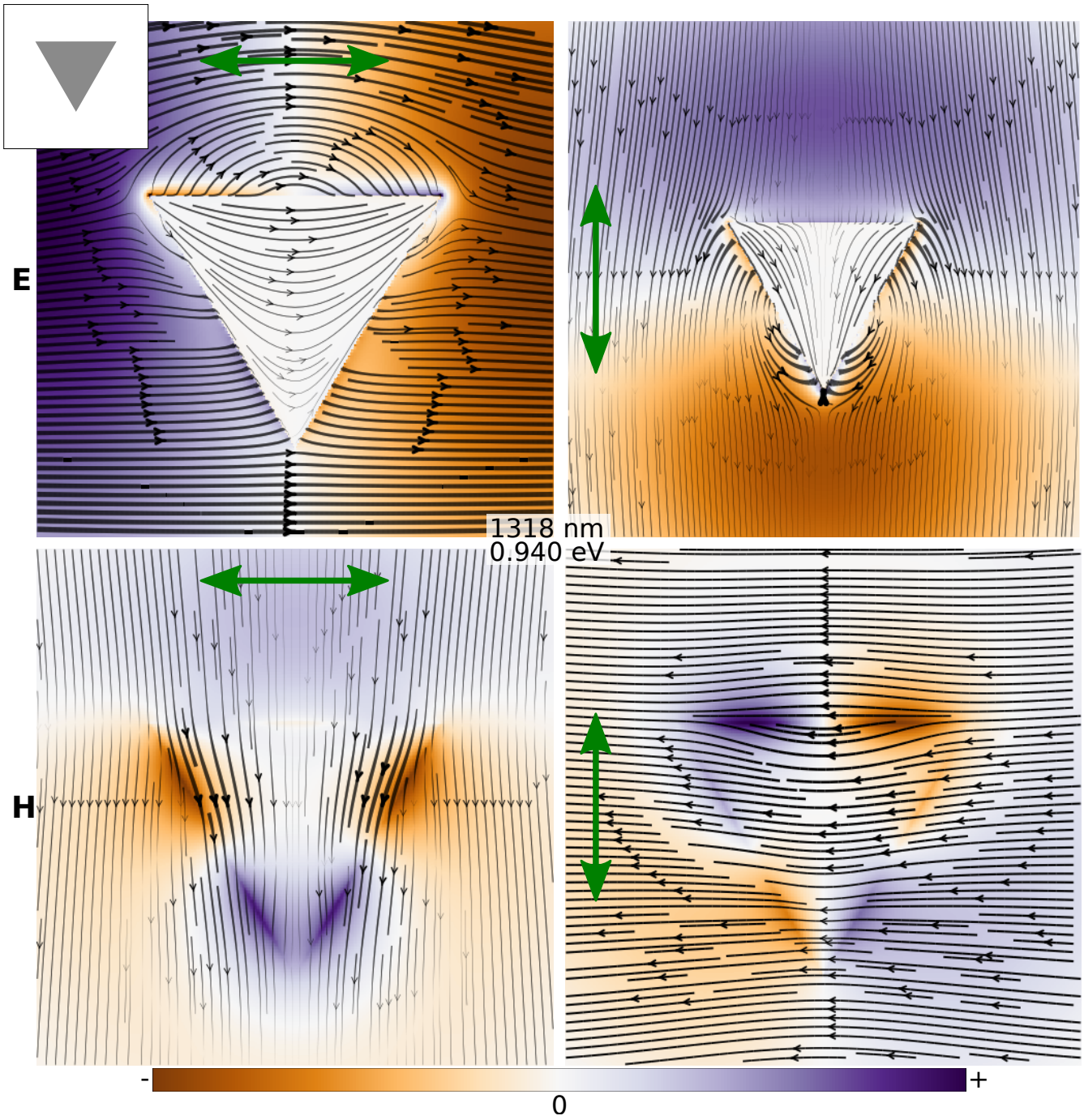

Figure S4: Simulated electric (**E**) and magnetic (**H**) fields for a plane just above the surface of the metal for a triangle (G0 structure, inset) at 0.94 eV (1318nm).

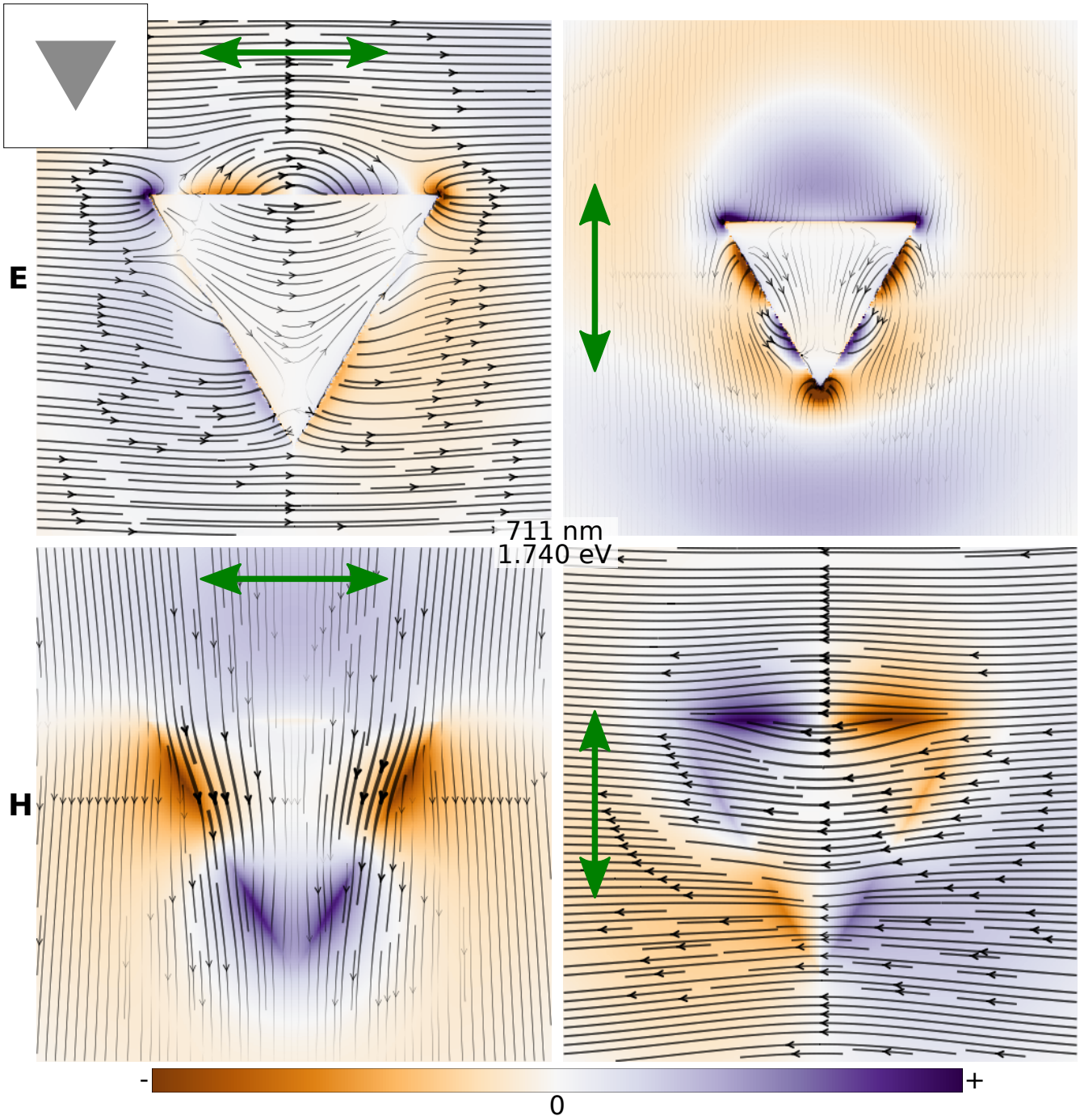

Figure S5: Simulated electric (**E**) and magnetic (**H**) fields for a plane just above the surface of the metal for a triangle (G0 structure) at 1.74 eV (711 nm).

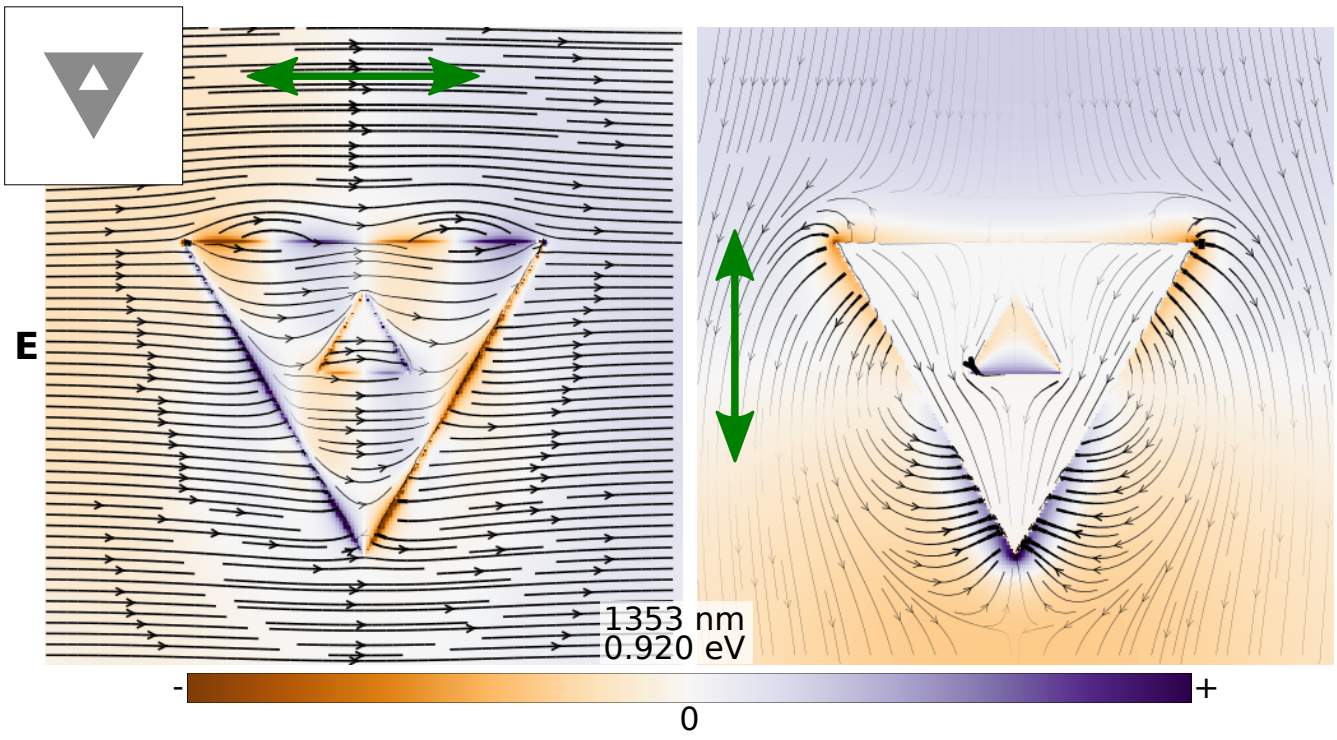

Figure S6: Simulated electric (**E**) fields for a plane just above the surface of the metal for a G1 fractal with a small aperture at 0.92 eV (1353 nm).

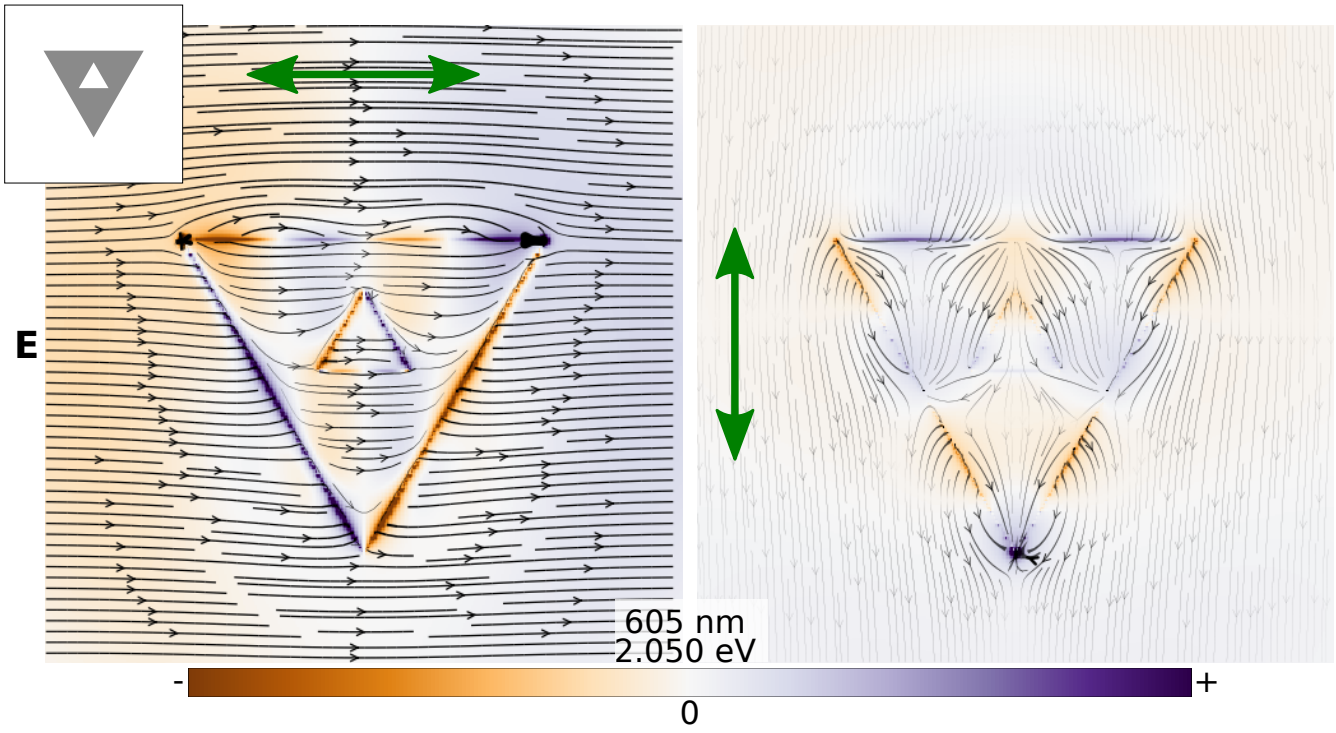

Figure S7: Simulated electric (**E**) fields for a plane just above the surface of the metal for a G1 fractal with a small aperture at 2.05 eV (605 nm).

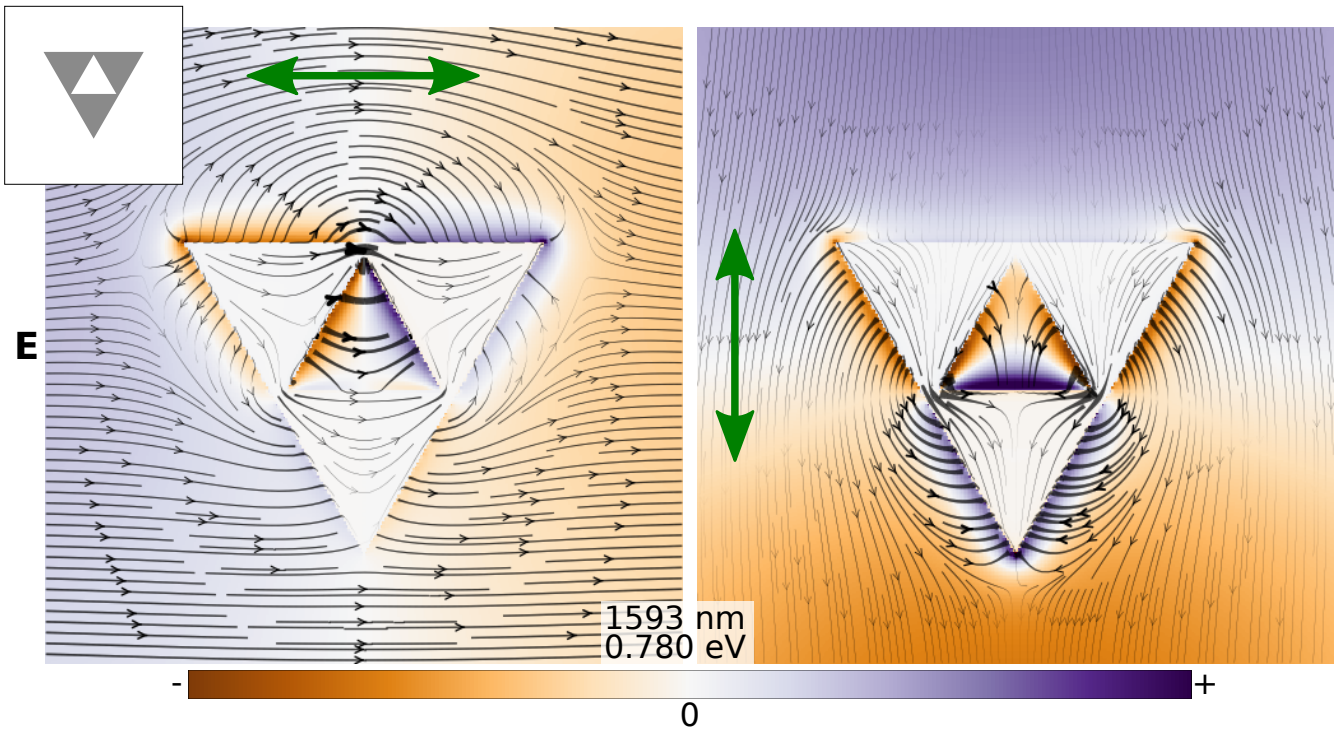

Figure S8: Simulated electric (**E**) fields for a plane just above the surface of the metal for a G1 fractal with a large aperture at 0.78 eV (1593 nm).

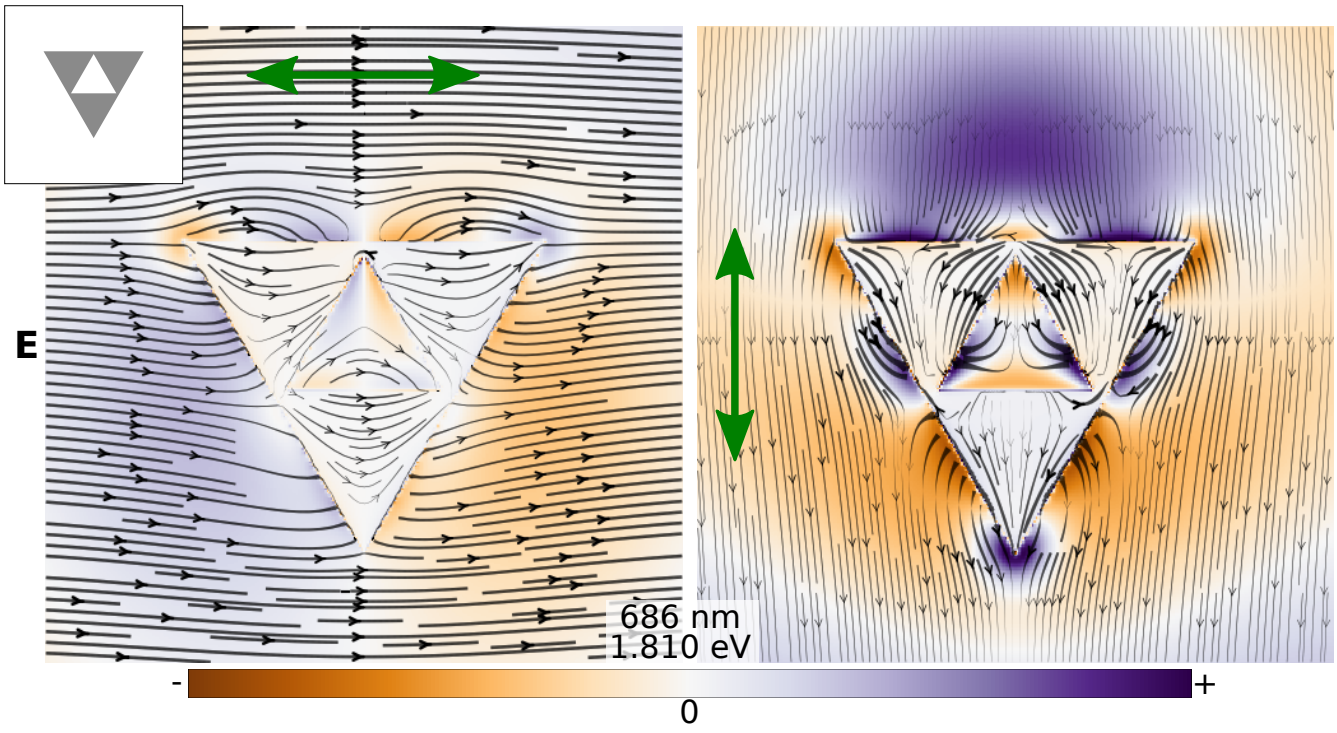

Figure S9: Simulated electric (**E**) fields for a plane just above the surface of the metal for a G1 fractal with a large aperture at 1.81 eV (686 nm).

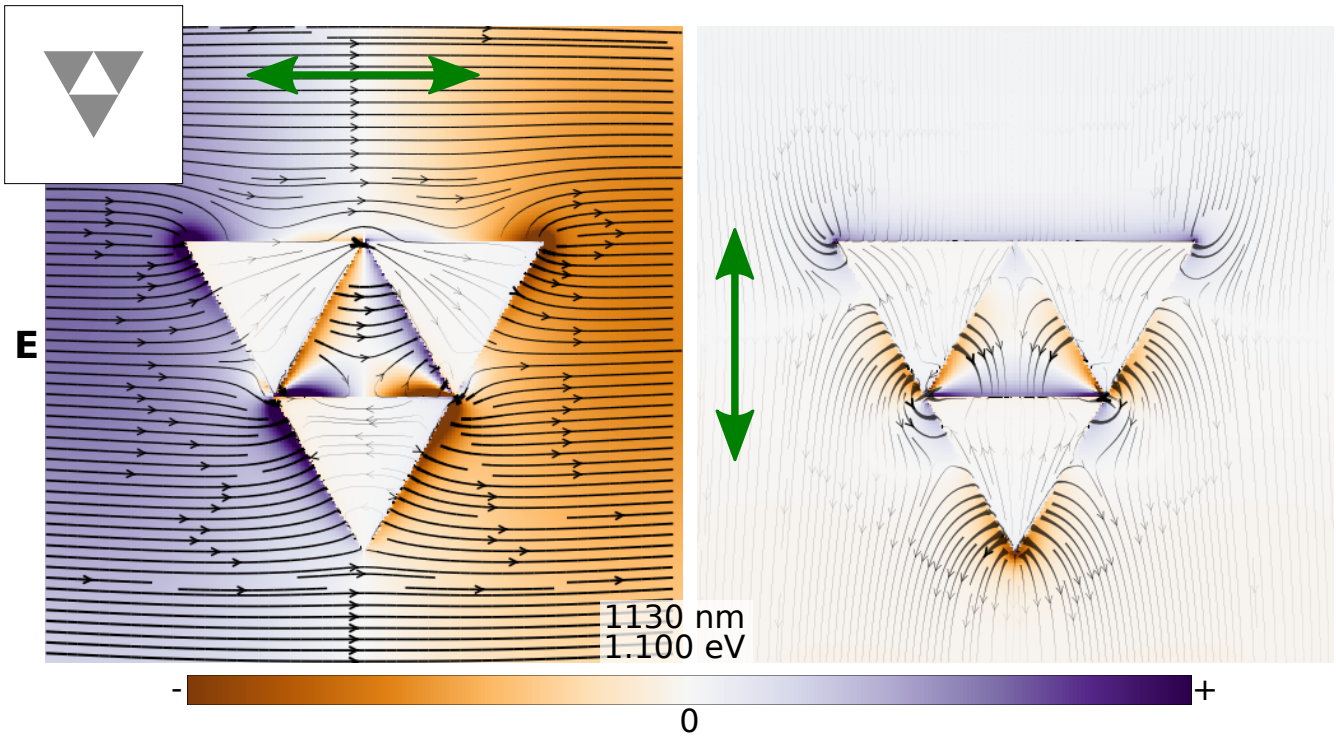

Figure S10: Simulated electric (**E**) fields for a plane just above the surface of the metal for a G1 fractal with a 'perfect' aperture, of the same size as the G0 parents, at 1.10 eV (1130 nm).

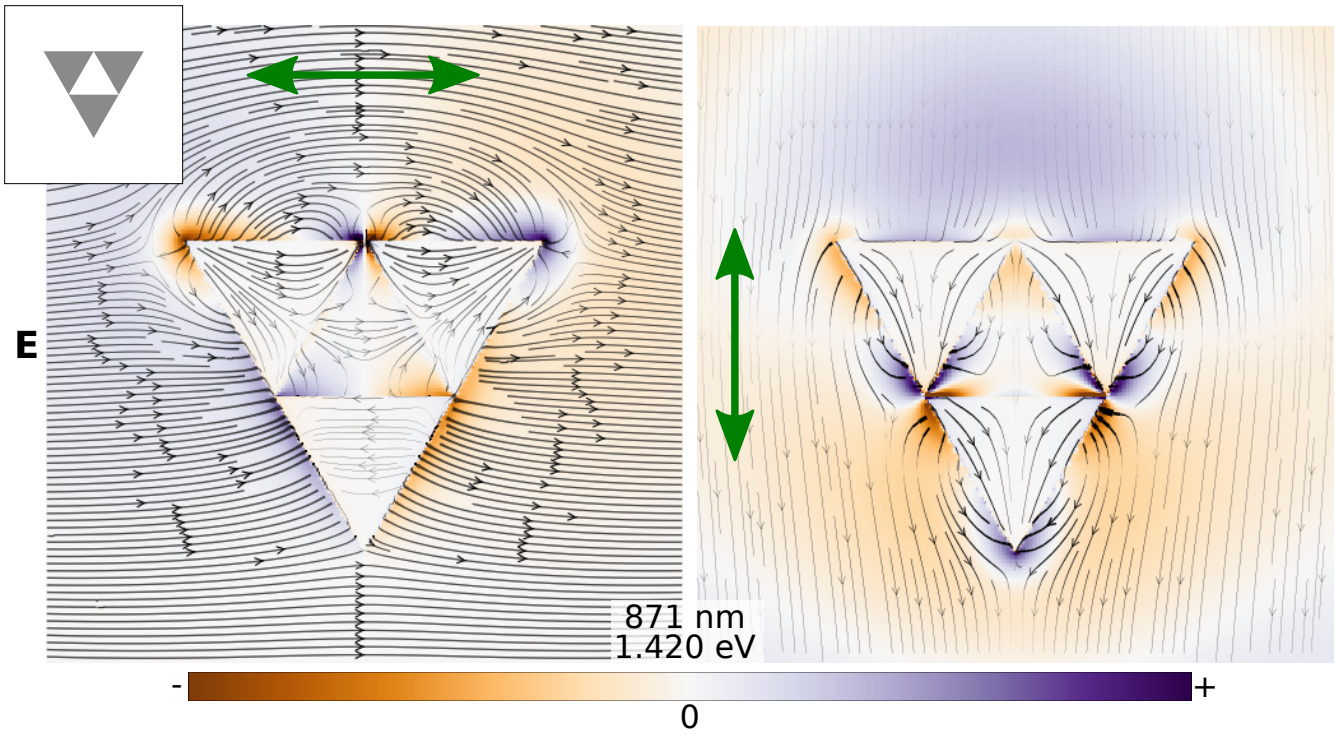

Figure S11: Simulated electric (**E**) fields for a plane just above the surface of the metal for a G1 fractal with a 'perfect' aperture, of the same size as the G0 parents, at 1.42 eV (871 nm).

Asymmetrical Babinet

In the case of the Sierpiński triangle, adding a triangular aperture into the middle of a G0 structure to create a G1 fractal does not change the symmetry of the overall structure. There are two orthogonal dipolar modes in the Sierpiński triangle for all fractal generations, assuming conductive coupling is maintained. To emphasize that each dipolar mode of the solid triangle is coupling to the orthogonal mode of the central aperture, the case where the symmetry is broken on introducing an aperture into a different structure is presented in Fig. S12. This example also highlights that the shifting of the modes caused by the addition of a central aperture is not unique to the fractal structure.

The two degenerate dipole modes of a simple silver square are shown in Fig. S12 A. Introducing a small square aperture into this square maintains the symmetry of the structure and degeneracy of the dipole modes, redshifting both equally (Fig. S12 B). A rectangular aperture introduced into the center of the square breaks the symmetry and the degeneracy of the dipolar modes on the new structure (Fig. S12 C,D). According to the Babinet principle, the lowest energy mode of the central aperture will couple to horizontally polarized light, orthogonal to the long axis of the aperture (the Babinet equivalent of a nanowire coupling to polarized fields along its length).[1,3] The vertical polarization, on the other hand, will couple to the aperture in the orthogonal direction, the equivalent of orthogonally polarized light coupling to the weaker transverse mode in a nanowire of the same dimensions as the aperture. Since the lower energy mode on the aperture is excited by fields polarized across the smallest dimension of the aperture, this mode couples to the horizontally polarized SPR mode of the square (Fig. S12 D) and the other mode, by similar arguments, couples to the vertically polarized SPR dipole mode (Fig. S12 C). The horizontally polarized case has a larger capacitance across the aperture than the vertically polarized case, resulting in a stronger redshift of the horizontal dipole mode. Alternatively, the coupling between the square dipolar mode and the slot dipolar mode is stronger in the case of the horizontally polarized SPR modes because of greater spectral overlap, presenting a greater redshift for

the more strongly coupled modes, as seen in Fig. S12.

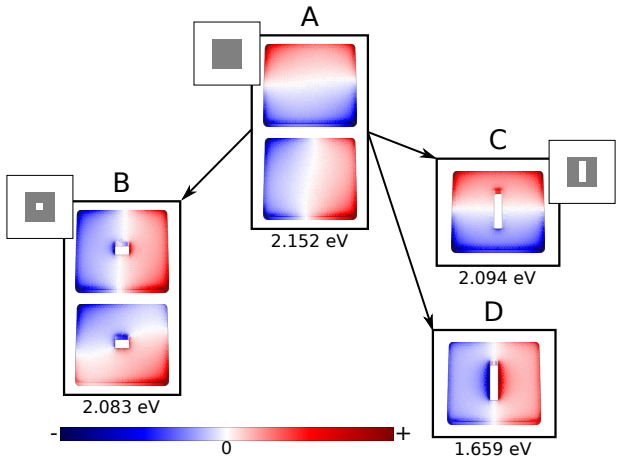

Figure S12: Dipolar eigenmodes for a silver square (A), a silver square with a small square aperture (B), and a silver square with a rectangular aperture (C, D).

Equivalent Circuits and the Degeneracy of the Dipolar Modes

The equivalent circuit theory applies concepts from resonant resistor-inductor-capacitor (RLC) electrical circuits to explain SPR mode behaviour. Simplified equivalent circuit diagrams[7] are presented in Fig. S13 for the dipolar modes of a G0 triangle; a G1 triangle with a small central aperture, allowing current to flow between G0 parent units; and a G1 fractal with a large central aperture which cuts off the conductive coupling between G0 parent units. Electrical sources are left out of the diagrams to maintain simplicity, since the sources will be approximately the same for all the structures presented. The top row of the figure represents a simplification of the flow of energy (blue and orange arrows for horizontally and vertically polarized excitation, respectively) through and around the structure, in the form of surface current or energy stored in capacitive fields across the central aperture or between the anti-nodes of the dipolar mode.

In the G0 triangle, the two dipolar modes (horizontally polarized dipole (HPD) and vertically polarized dipole (VPD)) are degenerate: they exhibit the same resonance energy, so must exhibit the same circuit characteristics. When the central aperture is introduced, it may be expected that the differences in conductive pathways across the device might cause splitting of the dipolar mode energies (Fig. S13(b)), but this is not the case. To explain this, the individual components of the equivalent circuit must be considered. For the VPD, the capacitance of the aperture might be expected to be higher than that for the HPD response, because of the larger area of the aperture when projected along the vertical direction, which should reduce the resonance frequency of the VPD mode relative to the HPD mode. However, the inductance along the conductive pathways also changes: for the VPD mode, both of the conductive paths around the aperture are narrower than those for the HPD mode. Narrower conductive junctions in the VPD results in a high self-inductance of each junction, resulting in an overall reduction in the circuit inductance via the addition

of two higher inductance values in parallel with the aperture capacitance. For the HPD, the capacitance may be lower than that of the VPD, but the inductance is higher because of the presence of one broad junction and one narrow junction around the central aperture. The lower circuit capacitance has the opposite effect on the position of the resonance as the higher inductance, which overall results in the same resonance frequency for both the HPD and VPD modes.

In the case where conductive coupling is broken (Fig. S13(c)), junction inductance does not appear in the equivalent circuit and the aperture capacitance is now in series with the resistance-inductance response of each of the smaller triangles in the fractal. Adding a series capacitor results in a blueshift of the dipolar modes and a splitting of the degeneracy (Fig. 3(c)(vi)). Capacitance across the triangular aperture is not equivalent in the two orthogonal directions.

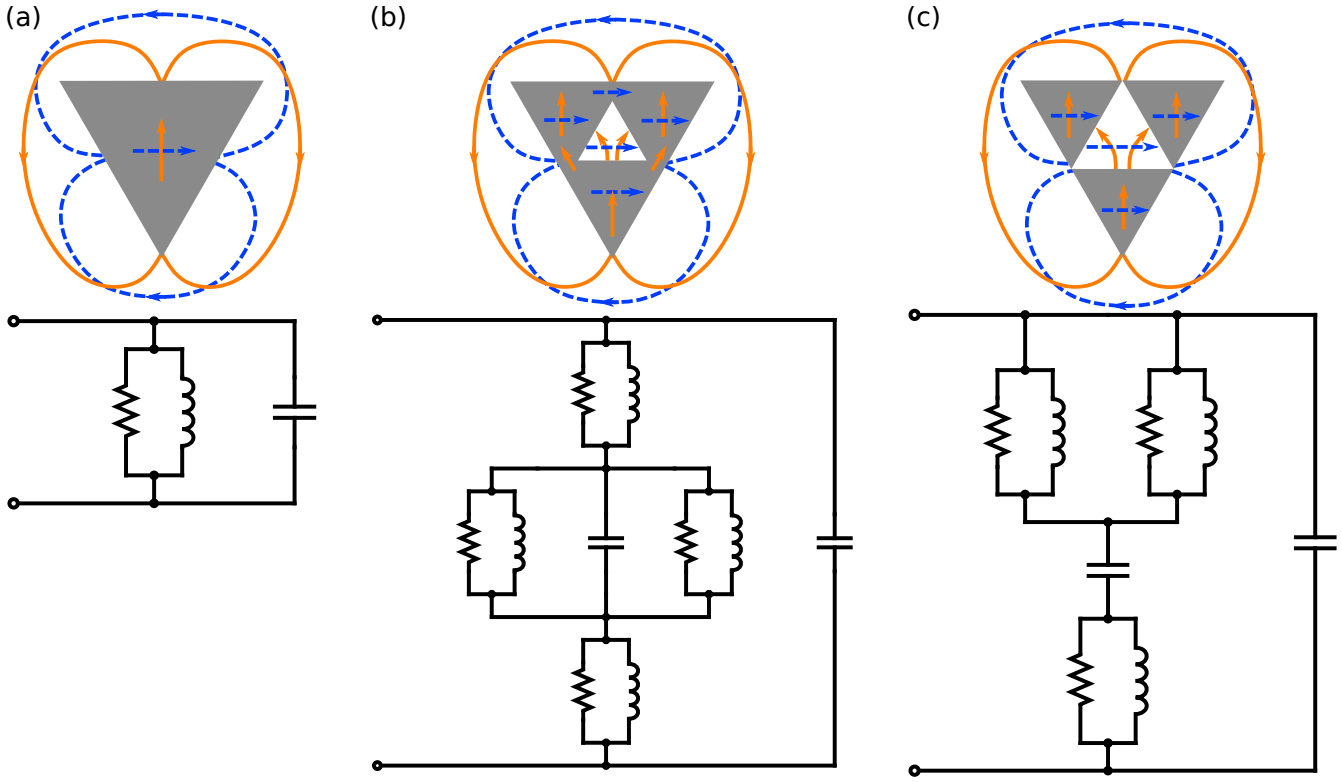

Figure S13: Simplified energy flow (top row) of the dipolar response to horizontally (blue arrows and vertically (orange arrows) polarized light and equivalent circuit diagrams (bottom row) representing the dipolar modes of (a) G0 triangle; (b) G1 fractal with a small aperture, maintaining conductive coupling between G0 parent units; and (c) G1 fractal with a large aperture, cutting off conductive coupling between parent units.

Linewidth Fitting

Calculation of the linewidth from the experimental EELS data was done using curve fitting provided by the Python Astropy library.[8] Raw spectra were averaged over the areas shown in Fig. S14, then deconvolved with 15 Richardson-Lucy deconvolution iterations. The three corners of each triangular structure were used to provide three datapoints in the fitting. A model composed of a power law and a Lorentzian peak was used to fit the zero loss peak tail and the dipolar plasmon peak within the energy region of the plasmon peak; the full width at half maximum of the Lorentzian function was taken as the linewidth of the plasmon peak. The results of the fitting are given in Fig. S14 and display a close fit for the energy range of interest.

The presence of the zero loss peak (ZLP) in an EELS experiment makes interpretation of the linewidth of a plasmon peak complicated: the ZLP is not only present as a large neighbouring peak with an extensive overlapping tail, but it is convolved with the signal from the sample. Richardson-Lucy deconvolution is an iterative procedure to deconvolve the ZLP from the sample signal, but the algorithm relies on an approximation to the point spread function (PSF) of the microscope system,[9] and does not perfectly remove the effect of the PSF from the acquired data. The linewidth of the dipolar plasmon peak was estimated for different numbers of deconvolution iterations, and it was found that although the values may still change as the number of iterations is increased (and deconvolution artifacts start to affect the results), the trend found between different structures remains the same. Contributions to the linewidth, even after several deconvolution iterations, include the PSF of the microscope and plasmon damping, which is strongly dependent on the fabrication and surface quality of the nanostructures. To improve the confidence that the modelled linewidth in the datasets is comparable, it is important to mention that all four samples were fabricated in parallel with each other, the EELS data was acquired on the same day using the same microscope conditions, and the same number of deconvolution iterations was performed using the same PSF reference spectrum.

For the fractals shown in Fig. 3, the 285 nm G0 fractal (a, b)(i) has a dipolar peak with a linewidth of 0.27 ± 0.04 eV; the G1 fractal with a small aperture (a, b)(ii) has a linewidth of 0.26 ± 0.03 eV on the dipolar peak; the G1 fractal with a larger triangular aperture (a, b)(iii) has a linewidth of 0.19 ± 0.015 eV on the dipolar peak; and the G1 fractal with the largest triangular aperture (a, b)(iv) has a linewidth of 0.19 ± 0.02 eV on the dipolar peak. The data exhibits a clear trend of reducing linewidth as the aperture size inside the G0 parent is increased.

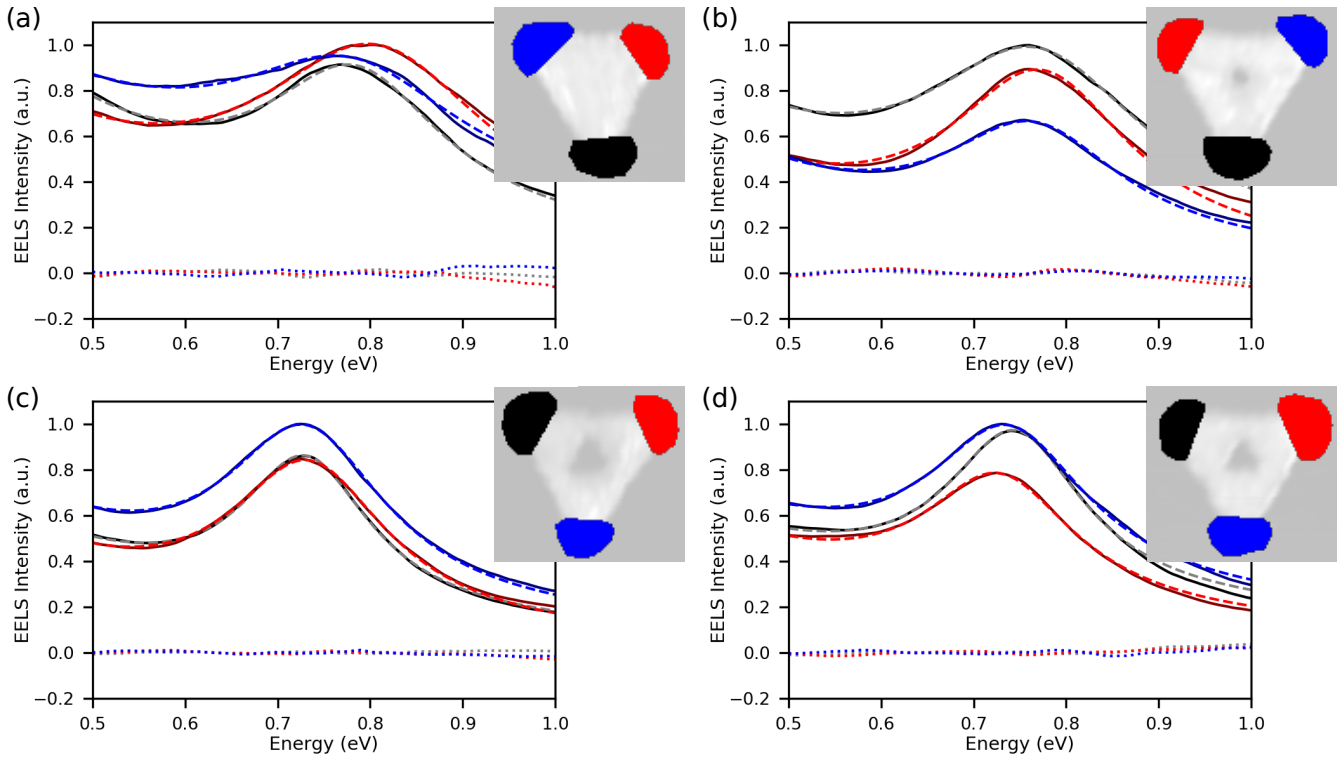

Figure S14: Fitting of a power law and Lorentzian model to the dipolar modes of G0 (a) and G1 (b,c,d) fractal triangles. Experimental EELS spectra were extracted from the areas coloured in the inset: solid lines are experimental data after 15 RL deconvolution iterations, dashed lines are the fitted model, dotted lines are the residuals of the fit for the respective colour.

FDTD Calculations of G2 and iG2

There are some differences between the experimental (Fig. 5) and simulated (Fig. 6) G2 and iG2 nanostructures; the EELS data shows the two lowest energy peaks of the iG2 structure framing the dipolar peak of the equivalently sized G2 triangle, whereas the simulated data presents two iG2 peaks at a higher energy than the dipolar modes of the equivalently sized G2 triangle. Examination of these trends provides an interesting case to apply the RLC circuit model. In both EELS and FDTD datasets, two peaks of approximately equal strength are observed at different energies. FDTD simulations reveal that these peaks correspond to excitation of the aperture mode across the large central aperture in the iG2 structure, and the excitation of aperture modes across the smaller apertures, respectively.

The key to understanding the difference in the energy relationship when compared to the G2 triangle is noticing that the conductive coupling across the structure is different between the experimentally fabricated iG2 structure and the simulated iG2 structure. In the fabricated iG2, the apertures are connected to each other and charge cannot flow in between the apertures, but must collect at the edges, acting as a capacitor, or flow around outsides of the smaller apertures. In the simulated structure, there is a conductive channel separating the large and small apertures, allowing charge to flow through this path. Similarly to the case of the G1 fractal, the conductive coupling across the structure greatly affects the energy of the modes. In the G1 case, when the conductive coupling is broken, the dipolar peak is blueshifted relative to the G0 of the same size; when the conductive coupling is broken in the iG2 structure, the dipole peaks are redshifted relative to the case with conductive channels. When the conductive channel between the smaller apertures and larger apertures is broken in the experimental iG2, charge is still able to flow around the outer edges of the small apertures, so the capacitance added by the extra gap should be considered as adding a capacitance in parallel with the rest of the equivalent circuit. Adding a capacitor in series increases the effective capacitance and reduces the resonant frequency, redshifting the dipole peak relative to the G2 triangle dipolar modes. In the simulated structure, there

is a conductive channel in between the small and large apertures, resulting in an overall lower capacitance for this structure and a higher energy dipolar mode.

Fig. S15 presents calculated electric fields for the two lowest energy peaks of a set of iG2 apertures in a solid silver film (iG2, spectrum (iv) in Fig. 6). The electric fields for the two lowest energy identifiable peaks in the G2 fractal response (see spectrum (iii) in Fig. 6) are presented in Fig. S16. For all plots, polarization of the excitation light is given by the green arrow. Streamlines indicate (x, y) field components and colours indicate the z component of the field for each plot.

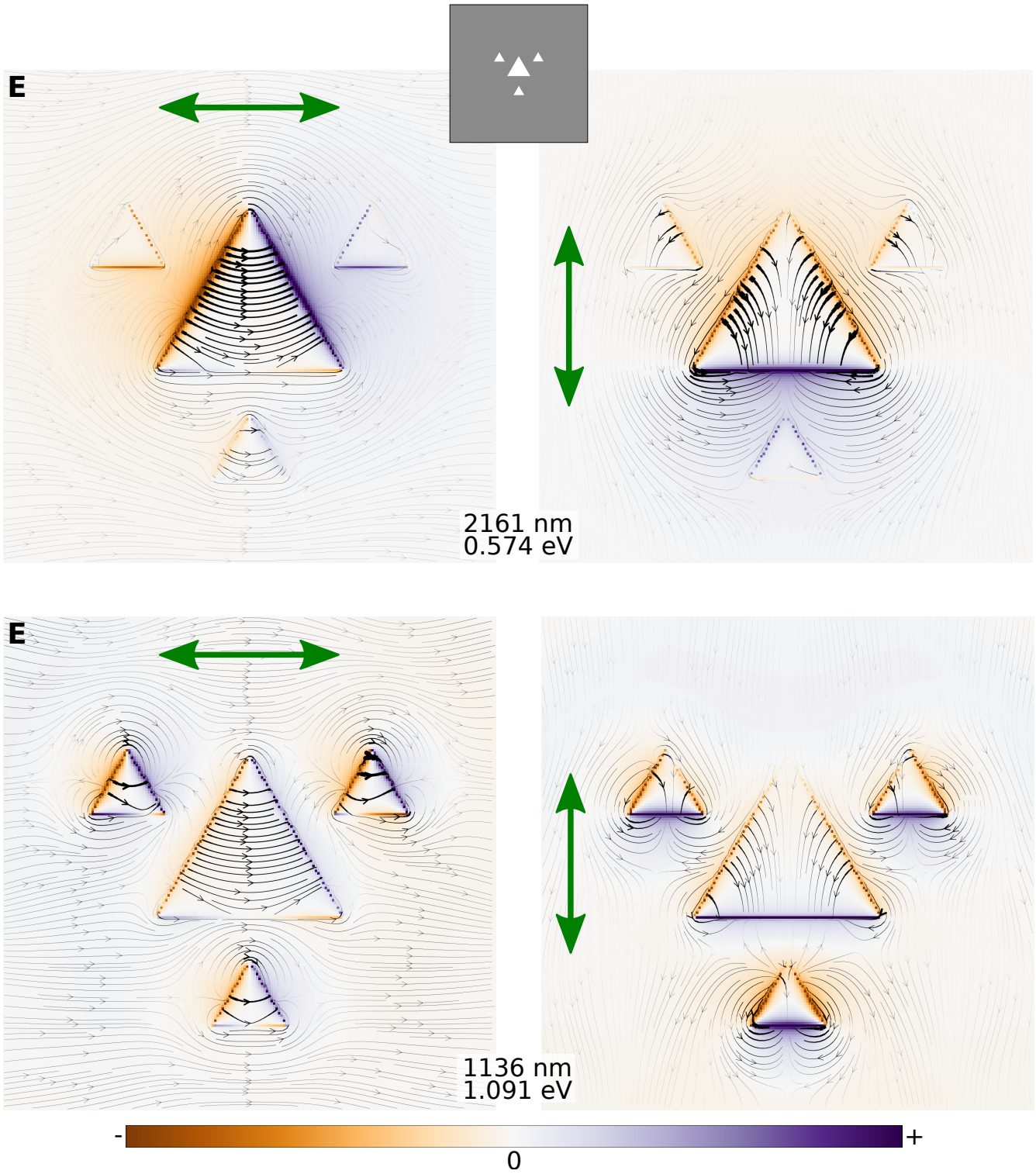

Figure S15: Simulated electric (**E**) and magnetic (**H**) fields for a plane just above the surface of the metal for a set of apertures corresponding to the apertures in a G2 fractal (iG2 structure) at 0.574 eV (2161 nm) and 1.091 eV (1136 nm).

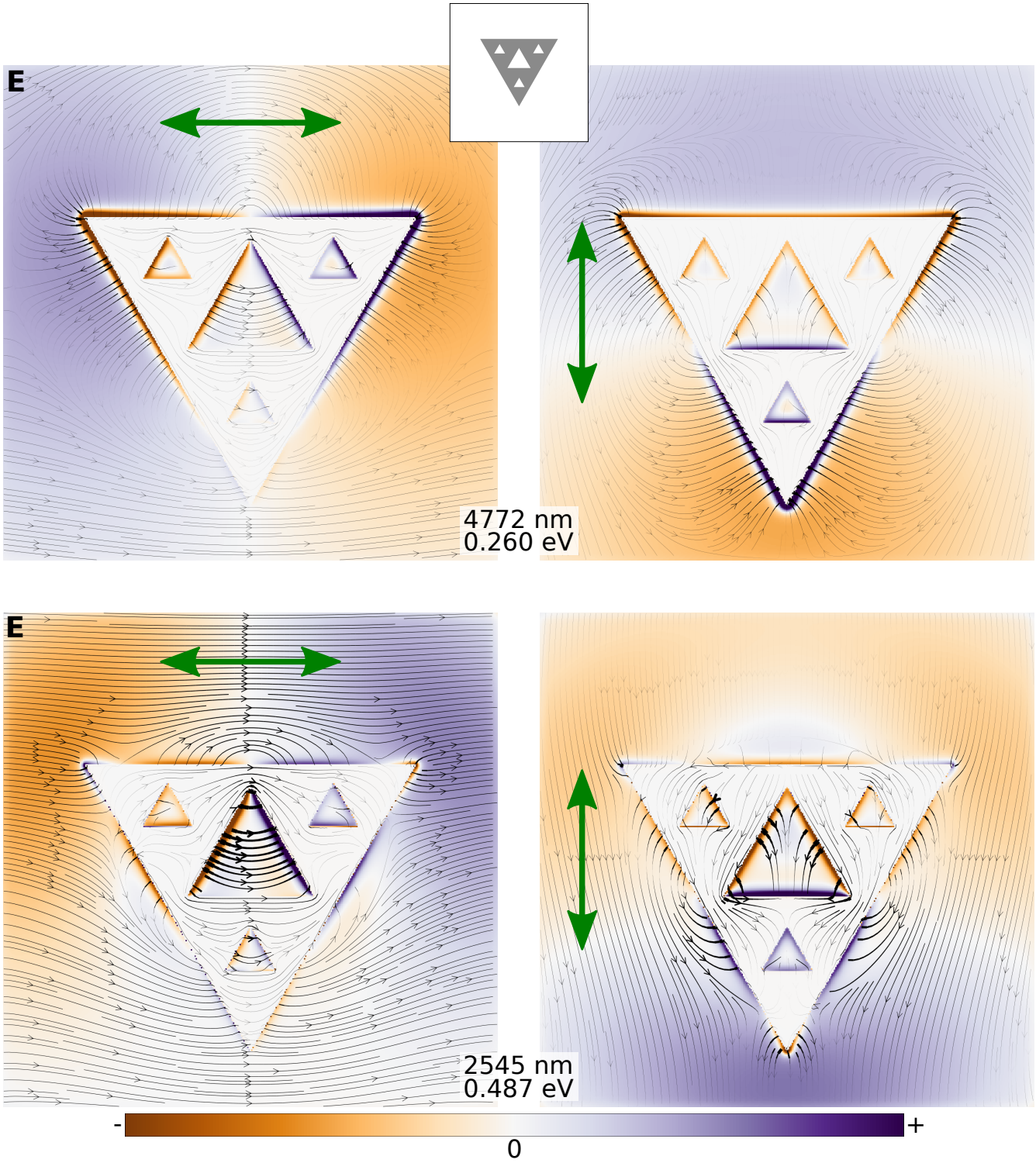

Figure S16: Simulated electric (**E**) fields for a plane just above the surface of the metal for a set of apertures corresponding to the apertures in a G2 fractal (iG2 structure) at 0.260 eV (4772 nm) and 0.487 eV (2545 nm).

References

(1) Booker, H. G. Slot aerials and their relation to complementary wire aerials (Babinet's principle). *J. Inst. Electr. Eng. Part IIIA* **1946**, *93*, 620–626.

(2) Hentschel, M.; Weiss, T.; Bagheri, S.; Giessen, H. Babinet to the Half: Coupling of Solid and Inverse Plasmonic Structures. *Nano Lett.* **2013**, *13*, 4428–4433.

(3) Rossouw, D.; Botton, G. A. Resonant optical excitations in complementary plasmonic nanostructures. *Opt. Express* **2012**, *20*, 6968–6973.

(4) Falcone, F.; Lopetegi, T.; Laso, M. A. G.; Baena, J. D.; Bonache, J.; Beruete, M.; Marqués, R.; Martn, F.; Sorolla, M. Babinet Principle Applied to the Design of Metasurfaces and Metamaterials. *Phys. Rev. Lett.* **2004**, *93*, 197401.

(5) Shuford, K. L.; Gray, S. K.; Ratner, M. A.; Schatz, G. C. Substrate effects on surface plasmons in single nanoholes. *Chem. Phys. Lett.* **2007**, *435*, 123–126.

(6) Zentgraf, T.; Meyrath, T. P.; Seidel, A.; Kaiser, S.; Giessen, H.; Rockstuhl, C.; Lederer, F. Babinet's principle for optical frequency metamaterials and nanoantennas. *Phys. Rev. B* **2007**, *76*, 033407.

(7) Engheta, N.; Salandrino, A.; Alù, A. Circuit Elements at Optical Frequencies: Nanoinductors, Nanocapacitors, and Nanoresistors. *Phys. Rev. Lett.* **2005**, *95*, 095504.

(8) Astropy Collaboration, et al. Astropy: A community Python package for astronomy. *Astron. and Astrophys.* **2013**, *558*, A33.

(9) Bellido, E. P.; Rossouw, D.; Botton, G. A. Toward 10 meV Electron Energy-Loss Spectroscopy Resolution for Plasmonics. *Micros. Microanal.* **2014**, *20*, 767–778.